View Article Online
DOI: 10.1039/C6RA13168A

Journal Name

ARTICLE

Impact of halogen-free flame retardant with varied phosphorus's chemical surrounding on the properties of diglycidyl ether of bisphenol-A type epoxy resin: synthesis, fire behaviour, flame-retardant mechanism and mechanical properties

Received 00th January 20xx,
Accepted 00th January 20xx

DOI: 10.1039/x0xx00000x
www.rsc.org/

Xiaomin Zhao,[a] Heeralal Vignesh Babu,[a] Javier Llorca,[a,b] and De-Yi Wang*[a]

Abstract This work aimed to investigate the effect of two types of phosphorus-containing flame retardants (P-FRs) with different chemical surroundings (phenylphosphonate-based (PO-Ph) and phenylphosphoric-based (PO-OPh)) on the flame-retardant efficiency for diglycidyl ester of bisphenol-A type epoxy (EP) resin. The two series of P-FRs which were named as FPx and FPOx (x=1, 2 and 3), respectively, showed reactivity with epoxy group that was examined by differential scanning calorimetric (DSC) and variable temperatures FTIR spectrum (VT-FTIR). A comparative study between the FPx and FPOx (x=1, 2 and 3) contaning flame-retardamt epoxy was carried out via investigating their flammability, thermal stability and mechanical properties. The most significant difference on flame retardancy between them was that FPx (x=1, 2 and 3) endowed EP with V-0 rating in UL 94 test at 5 wt% loading, while FPOx (x=1, 2 and 3) showed no rating at such loading. Importantly, it is found that there was almost 10 times difference in the flame-retardant efficiency for epoxy resin between FPx and FPOx, though they had similar chemically molecular structures. Moreover, TGA-FTIR and TGA-MS coupling techniques (TGA, thermalgravimetric analysis; MS, mass spectroscopy) were employed to study the thermal decomposition of FP1 and FPO1; the impacts of FP1 and FPO1 on the thermal decomposition of EP were studied by TGA-FTIR as well. Furthermore, an online temperature detection experiment was designed to collect the temperatures by thermocouple and infrared thermometers, respectively in the UL 94 test. Based on the above results, the flame-retardant mechanisms of FP1 and FPO1 in EP were discussed. In addition, the impact of P-FRs on mechanical properties of EP was studied by means of tensile test and dynamic mechanical analysis .

1. Introduction

1. Introduction

Epoxy resin, one of the most popular polymeric materials, plays indispensable role in many application fields, such as coating, transportation, electronic and electrical industrials (EE) due to its high performances on mechanical, electrical and chemical resistance. [1-3] Bifunctional diglycidyl ester of bisphenol A (DGEBA) based epoxy resins, are often utilized for semiconductor encapsulation in EE applications. A common curing agent for DGEBA is 4, 4- diaminodiphenylsulfone (DDS). Nevertheless, the intrinsic flammability of DGEBA/DDS is one of challenges for their products. [4-9] In past two decades, many research groups and industries devote themselves for improving flame retardancy of epoxy, such as halogenated flame retardants, nano-clays, organophosphorus compounds and polyhedral oligomeric silsesquioxane (POSS). [5-17] Generally, phosphorous containing flame retardants (P-FRs) are always regarded as one of the best choices to reduce flammability of epoxy resin since lots of halogenated flame retardants (H-FRs) are forbidden owing to their serious hazards for environment and human. [7-10]

9, 10-dihydro-9-oxa-10-phosphaphenanthrene 10-oxide (DOPO) and its derivatives are considered as most competitive phosphorus flame retardants for epoxy resin. [12-34] The addition of 6.3 wt% of DOPO to DGEBA/DDS reached high LOI value of 35%; however, the samples did not pass any rating in UL 94 test. [31] Recently, J. Artner et al. synthesized DOPO-based diaminic hardener for DGEBA/DDS carbon fiber reinforced composites. The LOI values of flame-retardant composites were increased by 17% and the UL 94 test results improved from a HB to a V-1 classification with around 1 wt% of phosphorus content.[12] Z. Li et al. found a good synergistic effect between polyhedral oligomeric octadiphenylsulfonylsilsesquioxane (ODPSS) and DOPO on flame-retardant epoxy resins. Epoxy with 2.5 wt% ODPSS and 2.5 wt% DOPO passed V-0 rating in UL 94 test. [32] More recently, it was reported that DGEBA/DDS system with 5 wt% of TNTP passed V-0 rating in UL 94 test. [33] Overall, most P-FRs reported in the above

[a] IMDEA Materials Institute, C/Eric Kandel, 2, 28906 Getafe, Madrid, Spain.
[b] Department of Materials Science, Polytechnic University of Madrid, 28040 - Madrid, Spain
* Corresponding author: De-Yi Wang (deyi.wang@imdea.org)
Electronic Supplementary Information (ESI) available: [details of any supplementary information available should be included here]. See DOI: 10.1039/x0xx00000x

View Article Online
DOI: 10.1039/C6RA13168A

literatures performed well in the flame retardant tests by means of large quantity of loading or higher content of phosphorous in epoxy resins. [12], [18], [20], [35] and [36]. In 2015, B. Schartel et al. proposed a two-step approach for condensed phase action to interpret the P-FR flame-retardant mechanism on two epoxy resins of DGEBA/DDS and RTM 6.[34] Since P-FRs has been regarded as very promising and effective non-halogenated flame retardant for polymers, in particular for epoxy resin, further understanding about the impact of phosphorus's chemical surrounding of P-FRs on the flame-retardant efficiency is very important to the development of high efficiency of flame retardant for epoxy resin.

This work mainly aimed to study the impact of phosphorus's chemical surroundings on the flame-retardant efficiency of P-FRs in EP (DGEBA-type epoxy resin/DDS). Two series of reactive P-FRs (Phenylphosphonate-based (PO-Ph) and phenylphosphoric-based (PO-OPh)) were synthesized with minor difference on the phosphorus's chemical surroundings. The two series of P-FRs were named as FPx and FPOx (x=1, 2 and 3), respectively. LOI, UL 94 and cone calorimeter tests were used to evaluate the impact of FPx and FPOx (x=1, 2 and 3) on improving flame retardancy of EP. In order to simplify the study, FP1 and FPO1 were chosen as one pair of representative to study the reactivity and flame-retardant mechanism of synthesized P-FRs in EP. First of all, the reactivity was characterized by means of heat flow curves in DSC test and variable temperatures infrared spectra of EPC, EPC/FP1 and EPC/FPO1 during 100 to 220 ^{o}C. One relative IR absorbance intensity ratios of R ($i_{(epoxy\ group)}/i_{(ether\ group)}$) were defined in order to described the changes of epoxy group during the heating. Aiming to understand the flame-retardant mechanism of FP1 and FPO1 in EP, a comprehensive research was done as followed: TGA-FTIR and TGA-MS coupling techniques were employed to study the evolved gaseous products of FP1 and FPO1 during thermal decomposition; the impact of FP1 and FPO1 on thermal decomposition of EP was studied by TGA-FTIR; an online temperature detection experiment was designed to record the samples temperatures near to surface and on surface by thermocouple and infrared thermometers respectively, aiming to describe the heat phenomena in UL 94 test. In addition, tensile and dynamic mechanical analysis (DMA) tests were used to evaluate the impact of P-FRs on tensile strength and viscoelastic properties of EP.

2. Experimental

2.1 Materials

Phenylphosphonic dichloride (PPDCl, 90%), phenyl dichlorophosphate (PDClP, 95%), allylamine (AA, 98%), n-octylamine (OA), 2-phenylethylamine (PA), diethyl ether, potassium bromide (KBr), triethylamine (TEA) and curing agent DDS were purchased from Sigma Aldrich Corporation. Epoxy resin (Brand name, EPC) (Epoxy equivalent, 0.54) was supplied by Faserverbundwerkstoffe® composite technology.

2.2 General procedure for synthesis of P-FRs

The modified general synthetic procedure of P-FRs was developed from Reference [38]. In a 500 mL three-neck flask, appropriate amine compound (AA, OA or PA) (0.21 mol) and TEA (0.2 mol) was dissolved in diethyl ether at 0-5 ^{o}C. Then a mixture of appropriate chloride compound (PPDCl or PDClP) (0.1 mol) and diethyl ether (100 mL) was added dropwise into the flask at 0-5 ^{o}C. The reaction mixture was stirred at 0-5 °C for 2 h. Then, stirring was continued for 5 h at room temperature (RT). After the reaction finished, the solid-liquid mixture was filtered off to remove triethylamine hydrochloride salt and the filtrate was evaporated under vacuum to obtain the crude product of P-FR. The product was purified by washing with deionized water for three times. In this work, PO-Ph FRs and PO-OPh FRs was named as FPx and FPOx (x= 1. 2 and 3), respectively, in order to simplify the name of synthesized P-FRs. Scheme 1 showed the synthetic routes and structures of FPx and FPOx (x=1, 2, and 3).

Synthesis of N, N'-Diallyl-P-phenylphosphonicdiamide (FP1)

Preparation of FP1 was followed the procedure described in 2.2 by using amine compound of AA (0.21 mol) and chloride compound of PPDCl (0.1 mol). FP1 was obtained as white solid. FR1: melting point (m.p.) 67 °C; yield, 80 %; ^{1}H-NMR (400 MHz, DMSO-d_6, δ) (ppm): 7.8-7.4 (Ar-H, 5H); 5.8 (=CH, 2H); 5.1- 4.9 (=CH_2, 4H); 3.4 (-CH_2-, 4H); ^{13}C-NMR (100 MHz, DMSO-d_6, δ) (ppm): 137.8, 135.5(134.3), 131.2, 127.8, 114.2, 42.4; ^{31}P-NMR (DMSO-d_6, δ) (ppm): 19.8.

Synthesis of N, N'-dioctyl-p-phenylphosphonicdiamide (FP2)

Preparation of FP2 was followed the procedure described in 2.2 by using amine compound of OA (0.21 mol) and chloride compound of PPDCl (0.1 mol). FP2 was obtained as white solid. FP2: m.p. 75 °C; yield, 80%; ^{1}H-NMR (400 MHz, DMSO-d_6, δ) (ppm): 7.7-7.4 (Ar-H, 5H); 2.7 (-CH_2(NH), 4H); 1.3-1.5 (-CH_2-, 12H); 0.8 (-CH_3); ^{13}C-NMR (100 MHz, DMSO-d_6, δ) (ppm): 136.8(135.2), 131.8, 131.1, 128.4, 44.4, 31.0, 28.2, 23.3, 22.0, 13.8; ^{31}P-NMR (DMSO-d_6, δ) (ppm): 20.4.

Synthesis of N, N'-di-phenylethyl-p-phenylphosphonicdiamide (FP3)

Preparation of FP3 was followed the procedure described in 2.2 by using amine compound of PA (0.21 mol) and chloride compound of PPDCl (0.1 mol). FP3 was obtained as a light yellow solid. FP3: m.p. 85 °C; yield, 85%; ^{1}H-NMR (400 MHz, DMSO-d_6, δ) (ppm): 7.7-7.2 (Ar-H, 15H); 2.7-3.1 (-CH_2, 8H); ^{13}C-NMR (100 MHz, DMSO-d_6, δ) (ppm): 140.4, 136.5(135.0), 131.8, 128.9, 126.6, 42.5, 38.7; ^{31}P-NMR (DMSO-d_6, δ) (ppm): 20.1.

Synthesis of N,N'-Diallyl-Phenylphosphoricdiamide (FPO1)

Preparation of FPO1 was followed the procedure described in 2.2 by using amine compound of AA (0.21 mol) and chloride compound of PDClP (0.1 mol). FPO1 was obtained as white solid. FPO1: m.p. 64 °C; yield, 95%; ^{1}H-NMR (400 MHz, DMSO-d_6, δ) (ppm): 7.4-7.0 (Ar-H, 5H); 5.9-5.7 (=CH, 2H); 5.2- 5.0 (=CH_2, 4H); 3.5-3.4 (-CH_2-, 4H); ^{13}C-NMR (100 MHz, DMSO-d_6, δ) (ppm): 151.6, 137.4, 129.2, 123.6, 120.5, 114.5, 43.1; ^{31}P-NMR (DMSO-d_6, δ) (ppm): 16.3.

View Article Online
DOI: 10.1039/C6RA13168A

Synthesis of N, N'-diamyl-p-phenylphosphoricdiamide (FPO2)

Preparation of FPO2 was followed the procedure described in 2.2 by using amine compound of OA (0.21 mol) and chloride compound of PDClP (0.1 mol). FPO2 was obtained as colorless liquid. FPO2: m.p. 73 °C yield, 95%; ^{1}H-NMR (400 MHz, DMSO-d_6, δ) (ppm): 7.7-7.4 (Ar-H, 5H); 2.6 (-CH_2(NH), 4H); 1.3-1.5 (-CH_2-, 12H); 0.9 (-CH_3); ^{13}C-NMR (100 MHz, DMSO-d_6, δ) (ppm): 152.5, 129.9, 124.1, 121.1, 41.3, 31.9, 29.5, 26.9, 22.7, 14.6; ^{31}P-NMR (DMSO-d_6, δ) (ppm): 20.4.

Synthesis of N, N'-di-phenylethyl-p-phenylphosphonicdiamide (FPO3)

Preparation of FPO3 was followed the procedure described in 2.2 by using amine compound of PA (0.21 mol) and chloride compound of PDClP (0.1 mol). FPO3 was obtained as yellow solid. PO-PA: m.p. 82 °C; yield, 95%; ^{1}H-NMR (400 MHz, DMSO-d_6, δ) (ppm): 7.4-7.1 (Ar-H, 15H); 2.7-3.1 (-CH_2, 8H); ^{13}C-NMR (100 MHz, DMSO-d_6, δ) (ppm): 152.3, 140.2, 129.9, 129.3, 128.9,124.3, 121.1, 43.1, 38.3; ^{31}P-NMR (DMSO-d_6, δ) (ppm): 13.9.

Preparation of epoxy of EP, EFPx and EFPOx (x=1, 2 and 3)

Epoxy reference (EP), EP/FPx (EFPx, x=1, 2 and 3) and EP/FPOx (EFPOx, x=1, 2 and 3) were prepared via a general procedure as below. First, appropriate amount of flame retardant P-FR (FP1-1, 3, 5 wt%; FPO1-1, 3, 5, 30 wt%; FP2 and FPO2-7.5 wt%; FP3 and FPO3-7.7 wt%) was mixed with EPC at 100 °C and stirred for 5 minutes. Then the stoichiometric amount of curing agent DDS was added slowly into EPC/P-FR mixture at 130 °C with stirring until DDS was totally dissolved. After this, the mixture of EPC/DDS/P-FR was poured into a pre-heated polytetrafluoroethylene (PTFE) moulds. The curing temperature profile was set as 160 °C for 1 h, 180 °C for 2 h and 200 °C for 1 h. The post curing process took place at 200 °C. The preparation of EP excluded the first step. All the compositions of EP, EFPx and EFPOx (x=1, 2 and 3) were listed in Tab. 1.

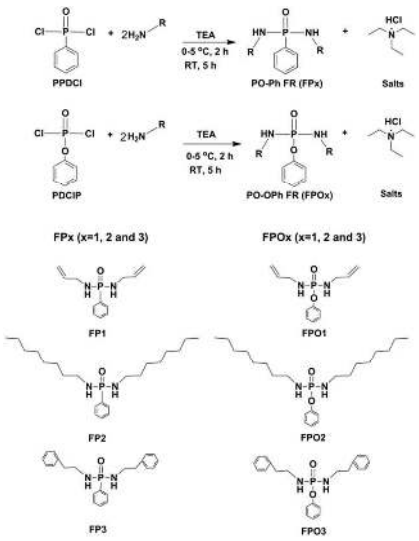

Scheme 1 The synthetic routes and structures of P-FRs (FPx and FPOx, x=1, 2 and 3)

2.3 Characterization

Nuclear magnetic resonance (NMR)

^{1}H, ^{13}C and ^{31}P NMR spectra were recorded on a Varian Mercury AS400 spectrometer at room temperature using DMSO-d_6 as solvent. The chemical shifts were reported in parts per million (δ) relative to tetramethylsilane (TMS) as a reference for ^{1}H and ^{13}C NMR (100 MHz). The ^{31}P NMR (162 MHz) spectra referenced to 85% H_3PO_4.

Differential scanning calorimetric (DSC)

DSC experiment was carried out on a DSC (Q200, TA) instrument under nitrogen atmosphere. 4-7 mg of samples was examined from 25 to 250 °C at a heating rate of 10 °C/ min.

Variable temperatures Fourier transform infrared spectroscopy (VT-FTIR)

Variable temperatures FTIR spectra were collected under a temperature-controlled heating device coupled with Nicolet iS50 FTIR spectrometer from 25 to 250 °C at a heating rate of 10 °C/ min. The liquid sample was dropped fully into the space between two pressed KBr disks. Then the two disks were put inside the heating sample holder and were imposed with a small force during the test. The scanning range for FTIR spectra was 4000-500 cm^{-1} with a resolution of 4 cm^{-1}. The sample was scanned 16 times and the sampling interval was 15.58 s. In this work, VT-FTIR test for each sample was repeated for three times. The results were well repeatable.

Flammability tests

LOI values of EP and flame-retardant EP were measured on oxygen index meter (Fire Testing Technology (FTT), UK) with precision of ±0.2 %. The sheet dimensions of the samples were 130×6.5×3.2 mm^3 according to ASTM D2863-97. Vertical burning tests were carried on a UL 94 Horizontal/Vertical Flame Chamber (FTT, UK) and sheet dimensions of the samples were 130×13×3.2 mm^3 according to ASTM D3801. Cone calorimeter test was carried out according to the ISO 5660-1 standard on a FTT cone calorimeter. Specimens with sheet dimensions of 100×100×3.2 mm^3 were irradiated at a heat flux of 50 kW/ m^2. Each sample were tested at least twice.

Scanning Electron Microscopy (SEM)

The morphology of char residues of EFP1-5 and EFPO1-5 after cone calorimeter test was tested by Scanning electron microscopy (SEM, EVO MA15, Zeiss, Germany). The samples were coated with a fine gold layer under 20 kV condition.

Thermal decomposition behaviors

Thermogravimetry coupled with Fourier transform infrared spectroscopy (TGA–FTIR): TGA (TA, Q50), interfaced with Nicolet iS50 FTIR spectrometer was used to characterize the evolved gas products during thermal decomposition of samples. 13±2 mg of samples was tested from room temperature to 700 °C at a heating rate of 10 °C/ min under the nitrogen flow. The decomposition products transferred through stainless steel line into the gas cell

View Article Online
DOI: 10.1039/C6RA13168A

under nitrogen carrier gas for FTIR detection. The transfer line and the gas cell were kept at 300 and 250 °C respectively to prevent the condensation of gaseous products. FTIR spectra recorded in a range of 4000–500 cm^{-1} with a 4 cm^{-1} resolution and averaging 16 scans. The sampling interval was 15.58 s.

The normal TGA test performed on the same instrument at a heating rate of 10 °C/ min. 5±1 mg of samples was examined under the air flow (90 ml/min) from room temperature to 800 °C.

Thermogravimetry coupled with Mass spectroscopy (TGA–MS): Mass spectrometer (Balzers (MS), MSC200) was connected with TGA in order to analyze the evolved gaseous during the thermal decomposition of flame retardants. 10±0.2 mg of sample was tested under argon and oxygen with a flow rate of 100 ml/min. The transfer lines between the TG and MS were heated to 250 °C in order to prevent the condensation of evolved gaseous.

Mechanical tests

Tensile test was measured on a Universal electromechanical testing machine (INSTRON 3384) at a rate of 0.5 mm/min. The cross-section dimension of dumbbell-shaped specimen was 4 mm × 4 mm and the length of testing was 35 mm. At least 5 specimens were tested for each sample in this study. Thermo mechanical properties were examined on a dynamic mechanical analyzer (DMA) (Q800, TA Instruments). The dimensions of sample were 35 mm × 10 mm × 2 mm. The samples were tested in a single cantilever clamp with a frequency of 1 Hz at a heating rate of 10 °C/min from room temperature to 240 °C.

3. Results and Discussion

3.1 Reactivity

DSC and VT-FTIR tests were employed to study the reactivity between N-H group on the structures of P-FRs and epoxy group in the structures of EPC. In this work, FP1 and FPO1 were chosen as one pair of representatives of FPx and FPOx (x=1, 2 and 3) for this study. The mole ratio of N-H group and epoxy group was stoichiometric ratio (1:1) for DSC and VT-FTIR tests.

The heat phenomenon of EPC and mixture of EPC/FP1 (or FPO1) occurred during the heating from RT to 220 °C were collected by DSC. (Fig. 1(A and B)) Meanwhile, VT-FTIR was used to show changes of IR absorbance intensity of epoxy group of EPC and mixture of EPC/FP1 (or FPO1) during the heating from RT to 220 °C. From VT-FTIR results, one relative IR absorbance intensity ratios of R ($i_{(epoxy\ group)}/i_{(ether\ group)}$) were defined in order to study the reactivity. (Fig. 1(B)) The ether group from the chain of epoxy resin was chemically stable during 100 to 220 °C whereas epoxy group reacted with N-H group from FP1 and FPO1 if the reactivity existed.

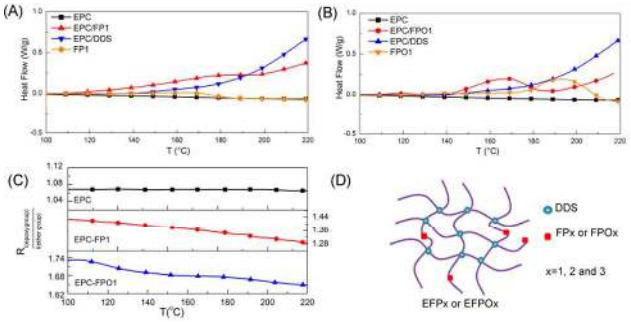

Fig. 1 A) DSC thermograms of EP, EPC/FP1, EPC/DDS and FP1; B) DSC thermograms of EP, EPC/FPO1, EPC/DDS and FPO1; C) R (i(epoxy group) / i(ether group)) vs temperature curves of EP, EPC/FP1 and EPC/FPO1 from VT-FTIR tests; C) Schematic structure diagrams of EFPx and EFPOx (x=1, 2 and 3)

In the heat flow curves in Fig. 1 A), EPC and FP1 did not show intensive heat phenomenon during RT to 220 °C. However, there was remarkable exothermic phenomenon since around 110 °C in DSC curve of EPC/FP1. Compared with the curing DSC curve of EPC/DDS, the exothermic phenomenon was also obvious. These results indicated that reaction occurred between FP1 and EPC. Furthermore, the R ratio of EPC was kept as stable value during the heating, whereas that of EPC/FP1 decreased since 110 °C in VT-FTIR test (Fig. 1(C)). The decreased R ratio was induced by the decrease of epoxy group. In view of the analysis of DSC and VT-FTIR results, N-H group on structure of FP1 was considered to be reactive with epoxy group. From Fig. 1B, EPC/FPO1 showed remarkable exothermic phenomenon since around 130 °C in DSC curve. Meanwhile, the R ratio also decreased in VT-FTIR test (Fig. 1C). The results showed that N-H group on structure of FPO1 was also reactive with epoxy group. Overall, the remarkable exothermic phenomena from DSC and the decreased R ratios from VT-FTIR results revealed that N-H group in the structures of synthesized P-FRs was reactive with epoxy group in the structures of EPC during 100 to 220 °C. FPx and FPOx (x=1, 2 and 3) were considered to be incorporated into EP by chemical bond linking. Fig. 1(D) described the schematic diagram of molecular chain structures for EFPx and EFPOx (x=1, 2 and 3) after curing with DDS. Such structures were supportive to avoid the leakage problem of flame retardant.

3.2 Flammability

LOI and UL 94 tests were used to evaluate the impact of FPx and FPOx (x=1, 2 and 3) on flammability of EP. The results were showed in Tab. 1 and the videos of UL 94 tests of EP, EFP1-5 and EFPO1-30 were uploaded in Supporting Information (Videos).

LOI of EP was 22 % and samples burnt out after 1st ignition in UL 94 test. The results revealed that EP was high flammable. In Tab. 1, FPx and FPOx (x=1, 2 and 3) showed similar impacts on EP in LOI test. LOI of EP was increased after the addition of both of them. However, the increase of LOI caused by the addition of FPx (x=1, 2 and 3) into EP was more significant than that caused by the addition of FPOx (x=1, 2 and 3). For instance, LOI of EFPO1-1 was 25% while

View Article Online
DOI: 10.1039/C6RA13168A

EFP1-1 was 28 %. EFP1-5 showed LOI of 31 % which was higher 9% and 4% than LOI s of EP and EFPO1-5, respectively. In addition, LOI of EFP3-7.7 was 37 % and was higher 3 % than that of EFPO3-7.7 which had the same P content of 0.67 wt% in the flame-retardant epoxy.

Significant impact induced by the addition of FPx and FPOx (x=1, 2 and 3) into EP was showed in UL 94 test. FPOx (x=1, 2 and 3) showed almost no impact on self-extinguishing ability of EP in UL 94 test within 5 wt% loading, whereas FPx (x=1, 2 and 3) endowed EP with strong self-extinguishing ability in UL 94 test even within 1 wt% loading. In UL 94 test, EFP1-1 self-extinguished the flame after 1st and 2nd ignition in UL 94 test although the burning time was above 10 s for each ignition. Moreover, the final burnt length was only 50±5 mm. In comparison with the total burnt of EP, EFP1-1 showed great reduction of fire propagation in UL 94 test. As P contents were fixed at 0.67 wt%, all EFPOx (x=1, 2 and 3) showed no rating, whereas all EFPx (x=1, 2 and 3) passed V-0 rating with short burnt length of 15±5 mm in UL 94 test. Notably, it found that until using 30wt% of FPO1 to epoxy (EFPO1-30) it can only pass V-1 rating, which was the same level as the EFP1-3.

Tab. 1 Results of LOI and UL 94 test of EP, EFPx and EFPOx (x=1, 2 and 3)

Samples	EPC/DDS (g: g)	P-FR [a] (wt%)	P [b] (wt%)	LOI (%)	UL 94	
					Rating	B.L.[d] (mm)
EP	100:34	0	0	22	NR[c]	130 (whole length)
EFP1-1	100:34	1	0.14	28	NR[c]	50±5
EFP1-3	100:34	3	0.40	29	V-1	40±5
EFP1-5	100:34	5	0.67	31	V-0	15±5
EFPO1-1	100:34	1	0.14	25	NR[c]	130(whole length)
EFPO1-3	100:34	3	0.40	26	NR[c]	130(whole length)
EFPO1-5	100:34	5	0.67	27	NR[c]	130(whole length)
EFPO1-30	100:34	30	4.00	28	V-1	40±5
EFP2-7.5	100:34	7.5	0.67	37	V-0	15±5
EFPO2-7.5	100:34	7.5	0.67	33	NR[c]	90±5
EFP3-7.7	100:34	7.7	0.67	37	V-0	15±5
EFPO3-7.7	100:34	7.7	0.67	34	NR[c]	100±5

a: Flame retardant content in epoxy; b: Phosphorus content in epoxy; c: No rating; d: burnt length

Above all, FPx (x=1, 2 and 3) showed significant different impacts on reducing flammability of EP compared with that FPOx did within small loadings. In the following research, FP1 and FPO1 were chosen as one pair of representatives of FPx and FPOx (x=1, 2 and 3) for further detailed research about the flame-retardant mechanism, respectively.

3.3 Fire behaviour

Cone calorimeter test was considered to be one of the most effective bench-scale tests to study the fire behaviours of polymer materials. Fig. 2 presented the characteristic curves of heat release rate (HRR) vs time (A) and mass vs time (B) of EP, EFP1-y and EFPO1-y (y=1, 3 and 5) from cone calorimeter test. The main performance parameters such as time to ignition (TTI), peak of heat release rate (pHRR), average of HRR (Avg. HRR), effective heat of combustion (EHC) and the residue at 500 s were listed in Tab. 2.

EP underwent intensive burning behaviour under cone heater at 50 kW/ m^2. After ignited around 55 s, the burning of EP was rapidly developed and terminated in short time. HRR of EP increased rapidly to pHRR of 1079 ±20 kW/m^2 in Fig. 2(A). This intensive combustion terminated within 300 s as shown in Fig. 2 (A). During the burning, EHC of EP was 22.0 ±1.5 MJ/kg. After cone calorimeter test, the residue of EP was around 9 ±3 wt% at 500 s, indicating that EP showed low charring ability to form protective char residue during fire behaviour.

From Fig. 2 and Tab. 2, the addition of FP1 and FPO1 in EP induced remarkable impact on the fire behaviour of EP. First of all, both HRR curves for EFP1-y and EFPO1-y (y=1, 3 and 5) showed two main peaks rather than one sharp peak from 50 to 500 s in Fig.2 (A). All the first peaks included shoulder peaks; the second peaks were broad and lower than 300 kW/m^2. In addition, both EFP1-y and EFPO1-y (y=1, 3 and 5) formed intumescent char residue in cone calorimeter test, as shown in S-Fig. 1 in Supporting Information. This type of char residue was beneficial for retarding heat and gaseous compounds exchanges between outer and inner of sample in cone calorimeter test. In Fig. 2(B), the weight loss of EFP1-y and EFPO1-y (y=1, 3 and 5) were depressed compared with that of EP, which was consistent with the changes of HRR curves. The similar impacts of FP1 and FPO1 on fire behaviour of EP were summarized as both EFP1-y and EFPO1-y (y=1, 3 and 5) showed shorter TTIs, lower pHRRs, lower Avg. HRRs and higher yields of residue at 500 s in comparison with EP did; the residue amounts of EFP1-y and EFPO1-y (y=1, 3 and 5) were similar after the test. Both of them

View Article Online
DOI: 10.1039/C6RA13168A

ranged from 20 ±2 wt% to 25 ±3 wt%, which increased 11 wt% -16 wt% in comparison with residue of EP.

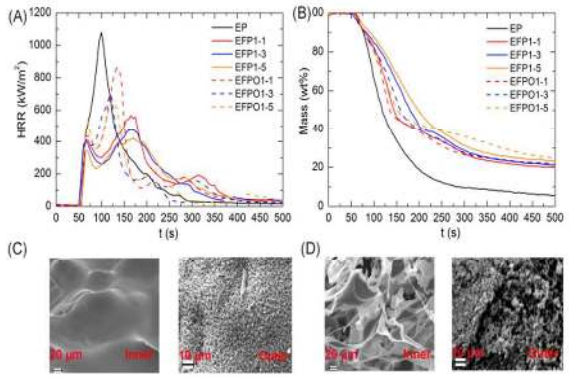

Fig. 2(A) Heat release rate (HRR) curves and (B) Mass curves of EP, EFP1-y and EFPO1-y (y=1, 3 and 5) as a function of time; (C) SEM images of inner and outer surfaces of EFP1-5 and (D) SEM images of inner and outer surfaces of EFPO1-5 after cone calorimeter test

Nevertheless interesting differences were specifically found between EFP1-5 and EFPO1-5. TTIs of EFP1-y (y=1, 3 and 5) were longer than those of EFPO1-y (1, 3 and 5) compared at the same loadings. For instance, TTI of EFPO1-5 was 50 ±2 s, lower 5 s than that of EP, while TTI of EFP1-5 was 55 ±3 s, keeping the same value with that of EP. In developed fire zone (52 s - 350 s), EFP1-y and EFPO1-y (y=1, 3 and 5) presented a shoulder peak on HRR curves in Fig. 2(A). The shoulder peak of EFPO1-y (y=1, 3 and 5) was sharp and terminated in short time within 20 s, while the shoulder peak of EFP1-y (y=1, 3 and 5) was broad and terminated within 45 s. Furthermore, HRR of EFPO1-y (y=1, 3 and 5) increased rapidly again after the shoulder peaks terminated. pHRR of EFPO1-5 was 702 ±35 kW/m^2. However, HRR of EFP1-y (y=1, 3 and 5) increased slowly after the shoulder peaks terminated. Until 175 s, pHRR of EFP1-y (y=1, 3 and 5) appeared with extremely low value in comparison with that of EP and EFPO1-5. pHRR of EFP1-5 was 419 ±47 kW/m^2 which was lower 61 % and 40 % than those of EP and EFPO1-5, respectively. In addition, the impacts of FP1 and FPO1 on EHC of EP were different. EFPO1-y (y=1, 3 and 5) showed EHC of 21.0±0.4, 21.5±0.6 and 20.5 ±0.5 MJ/kg, respectively. There was almost no change compared with that of EP. However, EHC of EP greatly decreased from 22.0±1.5 MJ/kg to 16.7±0.5 MJ/kg with 5 wt% loading FP1. It indicated that FP1 showed flame inhibition effect in the gas phase during the burning of EFP1-y (y=1, 3 and 5). Moreover, the mass losses of EFP1-y (y=1, 3 and 5) was slower than those of EFPO1-y (y=1, 3 and 5) during the test, although the residue amounts were similar at 500 s.

The shoulder peaks of EFP1-y and EFPO1-y (y=1, 3 and 5) were considered to be caused by the char residue formed after the sample was ignited. The formed char residue was able to delay the further decomposition of epoxy in limiting extension. In combination the different mass loss curves with the different pHRRs of EFP1-y and EFPO1-y (y=1, 3 and 5), it was indicated that the addition of FP1 endowed EP faster charring process that that of FPO1 in cone calorimeter test.

In addition, the morphology of inner and outer surfaces of the char residue of EFP1-5 and EFPO1-5 were characterized by SEM (Fig. 2 (C and D). Both the inner and outer surfaces of char residue from EFP1-5 were denser than those from EFPO1-5 after cone calorimeter test. It indicated that the char residue formed during fire behaviour of EFP1-5 was better for isolating effects than that of EFPO1-5 did.

Tab. 2 Data from cone calorimeter test of EP, EFP1-y and EFPO1-y (y=1, 3 and 5) at 50 kW/m^2

Sample	TTI[a] (s)	pHRR[b] (kW/m^2)	Avg. HRR[c] (kW/m^2)	EHC (MJ/kg)	Residue (500 s, wt%)
EP	55±2	1079±50	220±10	22.0±1.5	9±3
EFP1-1	54±3	600±45	200±9	20.2±0.6	20±2
EFP1-3	55±3	530±53	190±12	18.5±0.8	23±3
EFP1-5	55±3	419±47	171±15	16.7±0.5	24±2
EFPO1-1	54±2	864±57	208±6	21.0±0.4	22±3
EFPO1-3	52±2	720±52	189±11	21.5±0.6	23±3
EFPO1-5	50±2	702 ±35	173±13	20.5±0.5	25±3

a: time to ignition; b: peak of HRR; c: average of HRR;

3. 4 Thermal decomposition behaviour and flame retardant mechanism

In part 3.2 and 3.3, flame retardants FPx and FPOx (x= 1. 2 and 3) presented multiple impacts on flame retardancy of EP. In common, both the additions of FPx and FPOx (x= 1. 2 and 3) increased LOI of EP, decreased pHRR and accumulated the charring process of EP in cone calorimeter test. However, FPOx (x= 1. 2 and 3) showed almost no impact on self-extinguishing ability of EP, while FPx (x= 1. 2 and 3) endowed EP with strong self-extinguishing ability within small loadings in UL 94 test. In addition, FPx (x= 1. 2 and 3) increased LOI and decreased pHRR of EP in greater way than those FPOx (x= 1. 2 and 3) did. All these significant differences urged us to study the flame-retardant mechanism of EFPx and EFPOx (x= 1. 2 and 3). In this segment, FP1 and FPO1 were also chosen as one pair of representatives of FPx and FPOx (x= 1. 2 and 3).

3.4.1 Thermal decomposition of FP1 and FPO1

First of all, evolved gaseous products produced during thermal decomposition of FP1 and FPO1 were characterized via TGA-FTIR and TGA-MS.

Fig. 3 (A) and Fig. 4 (A) presented intensity variation of ion fragments with m/e of 78, 57, 41, 17, 66 and 94 detected by TGA-MS during the thermal decomposition of FP1. Fig. 3 (B) presented FTIR spectra of evolved gaseous products at different temperatures detected by TGA-FTIR during the thermal decomposition of FP1. Fig. 4 (B) presented absorbance intensity of IR peak at 923 cm^{-1} vs temperature curve from TGA-FTIR test of FP1.

From Fig. 3(A), allyamine, allyl and ammonium were the main evolved gaseous products from 200 to 350 ^{o}C during thermal decomposition of FP1. Ion fragments of benzene were detected

View Article Online
DOI: 10.1039/C6RA13168A

with m/e=78 since 350 °C. FTIR spectra showed in Fig. 3 (B) were mutual verified with these information.

Phosphorus-containing compounds were found with IR peak at 1260 cm^{-1} in FTIR spectra at 350 °C. Moreover, IR peak at 932 cm^{-1} gradually become notably in FTIR spectra at 450, 500 and 600 °C. This peak was assigned to P-O-P bond. Meanwhile, ion fragments with m/e=94 were detected since around 400 °C in TGA-MS test, as shown in Fig. 4 (A). It was not assigned to phenol ion fragment due to the lack signal of ion fragment with m/e=66. Combining the IR peak at 932 cm^{-1}, the fragments with m/e=94 were assigned to be from P_2O_2compound which had been reported by Lopez [39]. P_2O_2 was considered to be formed by radical PO· produced during thermal decomposition of FP1.

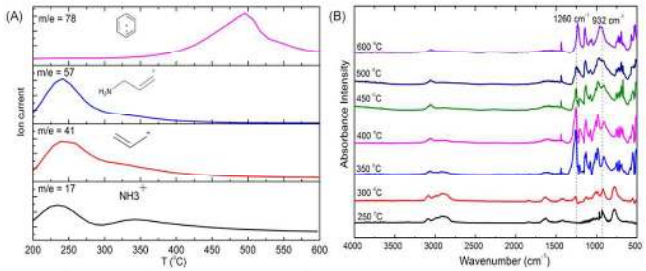

Fig. 3 (A Intensity variation of ion fragments with m/e =78, 57, 41 and 17 with temperature curves; (B) FTIR spectra at different temperatures of evolved gaseous products from thermal decomposition of FP1

Overall, P-N and C-N bonds on structure of FP1 were broken around 200 to 400 °C. Ammonium, allylamine and allyl compounds were formed and released into gas phase. Allyl compounds might also bonded again with phenylphosphonyl structure in condensed phase. The further decomposition of reformed structures in condensed phase produced complex mixture of gaseous products such as allyamine, benzene and phosphorus compounds. P (O)-Ph bond in FP1 structure dissociated nearly at 350 °C which was indicated by the release of benzene structure until 600 °C. Speculative thermal decomposition of FP1 was showed in Fig. 6(A). In condensed phase, phosphorous acid (H_3PO_3) was considered to be formed as shown in Fig. 6(A). [40]

Fig. 5 (A) presented intensity variation of ion fragments with m/e of 94, 66, 64, 57 and 41 detected by TGA-MS during thermal decomposition of FPO1. Fig. 5 (B) showed FTIR spectra of evolved gaseous products at different temperatures detected by TGA-FTIR of FPO1.

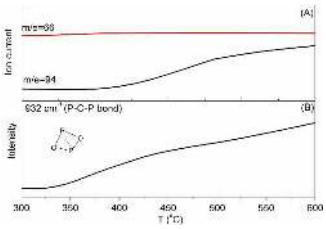

Fig. 4 (A): Intensity variation of ion fragments with m/e =66 and 94; (B): absorbance intensity variation of IR peak at 932 cm^{-1}

The thermal decomposition of FPO1 was different from that of FP1. From 200 to 400 °C, the detected ion fragments were mainly from phenol, allylamine and allyl compounds, as shown in Fig. 5 (A). Phenol ion fragments were detected until 550 °C. In Fig. 5(B), FTIR spectra at different temperatures were almost the simple added spectra of phenol and allyamine as shown in S-Fig. 2 in Supporting Information. From both TGA-MS and TGA-FTIR results, few signals from phosphorus compounds were detected in the evolved gaseous products. Only possible phosphorus compounds were considered to be metaphosphorous acid (HPO_2) which was assigned to the ion fragment with m/e=64 shown in Fig. 5(A). The above results indicated that phosphorus was mainly kept in condensed phase during thermal decomposition of FPO1. Speculative thermal decomposition path of FPO1 was showed in Fig. 6 (B). Phosphoric acid (H_3PO_4) was considered to be formed in condensed phase of FPO1 during thermal decomposition. [40] In case of FPO1, there was no significant signal indicating the formation of phosphorus radical at least during the main thermal decomposition of FPO1.

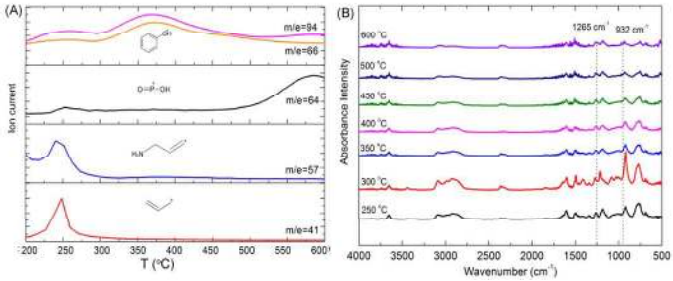

Fig. 5 (A) Intensity variation of ion fragments with m/e =94, 66, 57, 41 and 17 with temperature curves of FPO1; (B) FTIR spectra at different temperatures of evolved gaseous products from thermal decomposition of FPO1

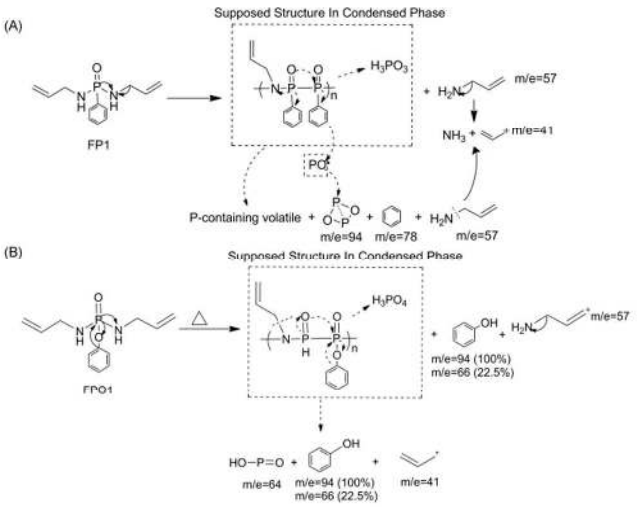

Fig. 6 (A): Speculative thermal decomposition rout of FP1; (B): Speculative thermal decomposition rout of FPO1

3.4.2 Thermal decomposition of EP, EFP1-5 and EFPO1-5

View Article Online
DOI: 10.1039/C6RA13168A

TGA-FTIR technique was employed to study the impact of FP1 and FPO1 on thermal decomposition of EP under nitrogen atmosphere. Fig. 7 (A) presented TGA curves of EP, EFP1-5 and EFPO1-5; (B) presented absorbance intensity of hydrocarbons as a function of temperature curves of EFP1-5 and EFPO1-5. In addition, the temperature at 5 % weight loss ($T_{d5\%}$), temperature at maximum decomposition rate (T_{max}) and residue at 600 ^{o}C of EP, EFP1-5 and EFPO1-5 were collected in S-Tab. 1 in Supporting Information. FTIR spectra of EP, EFP1-5 and EFPO1-5 at T_{max} were showed in S-Fig. 3 in Supporting Information.

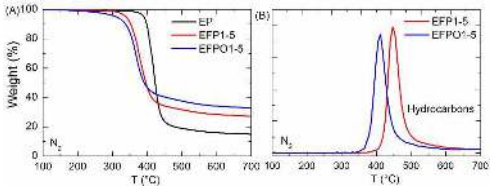

Fig. 7 (A): TGA curves of EP, EFP1-5 and EFPO1-5; (B) Absorbance intensity of hydrocarbons vs temperature curves of EFP1-5 ans EFPO1-5 from TGA-FTIR tests

Compared with TGA curve of EP, both the addition of FP1 and FPO1 brought $T_{d5\%}$ and T_{max} of EP to lower temperatures. Meantime, the char residue of EP was also increased at 600 ^{o}C, indicating that both FP1 and FPO1 accumulated the formation of char residues during thermal decomposition of EP. Seen from S-Fig. 3 in Supporting Information, FTIR spectra at T_{max} of EP, EFP1-5 and EFPO1-5 were very similar with each other, indicating that the addition of FP1 and FPO1 did not change the main decomposition rout of EP.

In detail, specific differences were found between TGA of EFP1-5 and EFPO1-5. $T_{d5\%}$ and T_{max} of EFP1-5 were 31 and 5 ^{o}C higher, respectively than those of EFPO1-5. The char residue of EFP1-5 was 27.8 %, while that of EFPO1-5 was 33.4 % at 650 ^{o}C. H_3PO_3 and H_3PO_4 formed during thermal decomposition of FP1 and FPO1 were considered to be effective for the formation of char residue during thermal decomposition of EFP1-5 and EFPO1-5, respectively. The different acidities of H_3PO_3 and H_3PO_4 were able to induce the formation of different char residue. Hydrocarbons from thermal decomposition of polymer materials were regarded as the main "fuel" to be ignited under heating or fire exposure.[8] Fig. 7(B) showed that hydrocarbons produced from thermal decomposition of EFPO1-5 started to be detected since 350 ^{o}C, while those produced from thermal decomposition of EFP1-5 started to be detected since 400 ^{o}C.

3.4.3 Flame retardant mechanism

In combination 3.4.1 analysis about thermal decompositions of FP1 and FPO1 with 3.4.2 analysis about thermal decompositions of EFP1-5 and EFPO1-5, flame-retardant mechanisms of FPx and FPOx (x=1, 2 and 3) in EP was proposed as below.

In condensed phase, FP1 and FPO1 acted on burning of EP in the same way. The typical intumescent components formed in both EFP1-5 and EFPO1-5 under heating or igniting: the acid compounds (H_3PO_3 and H_3PO_4) from thermal decomposition of FP1 and FPO1 acted as acid sources; EP matrix acted as char former; the gaseous products from thermal decomposition of EFP1-5 and EFPO1-5 acted as blower. Foam-like char residues were observed both in EFP1-5 and EFPO1-5 during cone calorimeter test. The char residue acted as a physical barrier that slowed down heat and gaseous products transfer between inner and outer of matrix.

However, the release temperature of acid compounds and evolved gaseous products and the charring rate of epoxy matrix affected the formation of foam-like char residues. For instance, char residue of EFP1-5 was denser than that of EFPO1-5, even their mass and the intumescent shape were similar with each other. As seen from Fig. 2 (B), EFP1-y (y=1, 3 and 5) showed fewer mass loss than EFPO1-y (y=1, 3 and 5) did before 200 s in cone calorimeter test. The similar thing occurred before 400 ^{o}C in TGA test, shown in Fig. 7 (A). It indicated that the charring rate of EFPO1-y (y=1, 3 and 5) was lower than that of EFP1-y (y=1, 3 and 5) at initial stage under heating. In addition, the density of char residue from EFP1-5 was higher than that from EFPO1-5. The two differences induced the lower pHRRs for EFP1-y than those of EFPO1-y (y=1, 3 and 5) in cone calorimeter test.

View Article Online
DOI: 10.1039/C6RA13168A

Journal Name

ARTICLE

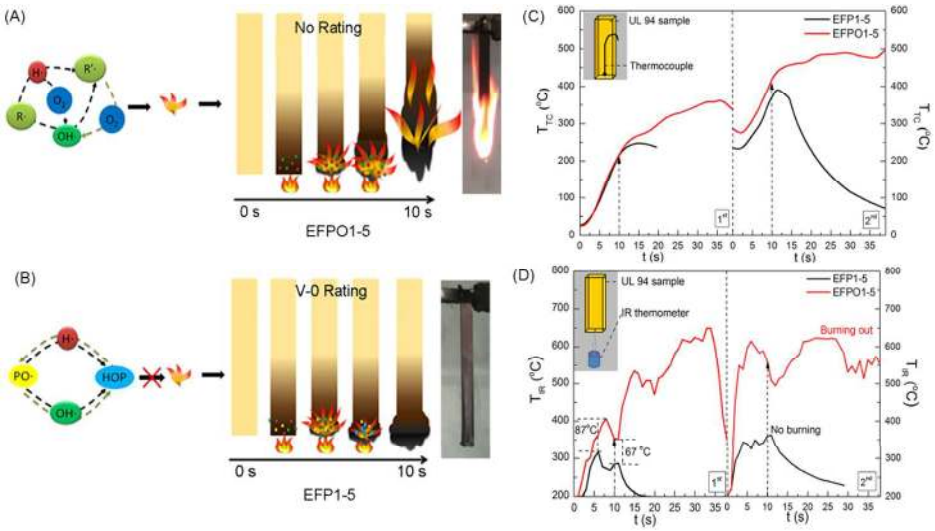

Fig. 8 Fig. 8 Proposed gas phase effect and burning scheme of EFPO1-5 (A) and EFP1-5(B) in UL 94 test; (C) T_{TC} vs time curves of EFP1-5 and EFPO1-5 in UL 94 test; (D) T_{IR} vs time curves of EFP1-5 and EFPO1-5 in UL 94 test

In gas phase, FPO1 showed no significant impact, while FP1 showed efficient flame inhibition effect on burning of EP. As to FPO1, firstly, the dilution effect was not presented due to the small loading of FPO1 and the minor impact of FPO1 on thermal decomposition of EP. Secondly, there was no active moiety and radicals that was able to capture H· and OH· radicals to interrupt the combustion chain during thermal decomposition of FPO1. The gas phase action of FPO1 was speculatively described in Fig. 8 (A).

As to FP1, hydrocarbons released around 400 ^{o}C for EFP1-5，indicating that H· and OH· were continuously generated since then. The radical reactions involved with these two kinds of radicals greatly impact the burning velocity of EFP1-5. However, FP1 produced PO· radical when thermal decomposed. PO· radical was able to annihilate H· and OH· as shown in Fig. 8 (B). The concentrations of H· and OH· lowered down owing to the annihilate effect, meaning that the radical flame reaction cycle was depressed.

In recent years, researchers made a lot of efforts to study the specific fire behaviour in different tests, such as LOI, UL 94 and cone calorimeter tests. [41, 42] In this work, the near-to-surface temperature (NTST) and surface temperature (ST) of UL 94 test samples of EFP1-5 and EFPO1-5 were collected by thermocouple thermometer and infrared thermometer (IR thermometer), respectively, as shown in Fig.8 (C and D). During the experiment, the emissivity was always set as 0.950 for IR thermometer. The T_{TC} (NTST) vs time and T_{IR} (ST) vs time curves of EFP1-5 and EFPO1-5 were showed in Fig. 8 (C and D).

In Fig. 8(C), T_{TC} of EFPO1-5 increased continuously during no matter 1st or 2nd 10 s ignition in UL 94 test. At 1st 10 s, T_{TC} of EFPO1-5 was 215 ± 15 ^{o}C and that of EFP1-5 was 211 ± 14 ^{o}C. Meantime, their slopes of T_{TC} curves were very close to each other. After the 1st 10 s ignition, T_{TC} of EFPO1-5 continued increasing until 35 s when the flame was out, while T_{TC} of EFP1-5 decreased within 5 s after 10 s. During the 2nd 10 s ignition, the rising rates of T_{TC} curves were also in the similar level for EFPO1-5 and EFP1-5. After 2nd 10 s ignition, T_{TC} of EFPO1-5 increased around to 500 ^{o}C and kept relatively stable value until the burning finished. However, T_{TC} of EFP1-5 decreased within 3 s after 2nd 10 s ignition. The trends of T_{TC} curves were consistent with the burning behaviour: EFPO1-5 burnt more than 10 s, while EFP1-5 burnt within 5 s no matter after 1st or 2nd ignition.

In Fig. 8 (D), interesting differences of T_{IR} between EFP1-5 and EFPO1-5 were showed. Both EFP1-5 and EFPO1-5 presented up-down trend during 1st and 2nd ignition. However, the increase of T_{IR} of EFP1-5 slowed down when T_{IR} was 300 ± 40 ^{o}C, whereas that of EFPO1-5 slowed down when T_{IR} was 400 ± 40 ^{o}C during 1st 10 s ignition. The maximum difference between T_{IR}s of EFP1-5 and EFPO1-5 was around 80 ^{o}C during 1st ignition. During 2nd 10 s ignition, T_{IR}s of EFPO1-5 and EFP1-5 increased in the same way at first. However, T_{IR} of EFP1-5 did not increase obviously when the value was around 350 ± 40 ^{o}C. T_{IR} of EFPO1-5 increased to 550 ± 40 ^{o}C until the 2nd 10s ignition. The maximum difference was up to 300 ^{o}C during 2nd ignition. In the following time, T_{IR} of EFPO1-5

View Article Online
DOI: 10.1039/C6RA13168A

increased around to 600 °C until the burning finished, while that of EFP1-5 decreased immediately when the flame was out.

Basically, the heat energy to increase T_{IR} (Q_{ST}) was described as following equation: $Q_{ST} = Q_F+Q_B-Q_D-Q_C$. Q_F represented the heat from UL 94 test flame; Q_B represented heat from burning of sample; Q_D represented the decomposition heat from samples; Q_C represented the conductive heat of sample. Herein, we assumed that Q_D were same for the two systems.

From the T_{TC} vs time curves, it was noted that T_{TC} of EFP1-5 and EFPO1-5 showed almost the same rising rate during 1st and 2nd ignition. It was indicating that Q_C was considered the same for two systems as well. Under such hypothesis, Q_{ST} only depended on value of Q_B, because Q_F had been also controlled in the same way. According to Fig. 8 (D), obviously, Q_B of EFPO1-5 was much higher than that of EFP1-5. It meant that the burning of EFP1-5 was much weaker than that of EFPO1-5, which was attributed by the flame inhibition effect of PO· in gas phase.

As a whole, the following two factors induced high efficient flame retardancy of FP1 on EP: (i) flame inhibition effect in gas phase; (ii) catalyzing charring process in condensed phase. We believed that flame inhibition effect was the main factor to endow EP with strong self-extinguishing ability. Due to a combination of flame inhibition and catalyzing char formation effects, FP1 induced V-0 rating in UL 94 test, high LOI value and low HRR for EP at very low loading. It also fit to explain the fire behaviours of other FPx (x=1, 2 and 3) containing flame-retardant epoxy.

3.5 Mechanical Properties

Strain-stress curves, tensile strength and Young's modulus charts of EP, EFP1-5 and EFPO1-5 were showed in Fig. 9 (A and B). Storage modulus curves and loss factor (Tan δ) curves were displayed in Fig. 9 (C and D) from dynamic thermo mechanical analysis (DMA). The addition of FP1 and FPO1 did not present significant impact on tensile behaviour of EP as shown in Fig. 9(A). The tensile strengths of EFP1-5 and EFPO1-5 were lower within 5 % compared with that of EP. (Fig. 9(B)) It meant that the impact of FP1 and FPO1 on tensile strength of EP was negligible. Young's modulus of EP was 1911 ±65 MPa. It was increased to 2103 ±60 and 2107 ± 75 MPa after the addition of FP1 and FPO1 respectively, indicating that the addition of FP1 and FPO1 slightly increased the rigidity of EP.

The results of dynamic thermo mechanical analysis in Fig. 9(C and D) showed that the impacts of FP1 and FPO1 on viscoelastic property of EP were also negligible. Either on glass state or rubbery state, storage modulus of EFP1-5 and EFPO1-5 showed in the same magnitude with that of EP. In addition, the peak of Tan δ was used to evaluate the glass transition temperature (Tg) in this work. Tg of EP was 187 ±3 °C, whereas those of EFP1-5 and EFPO1-5 were also 187 ±4 °C respectively. Fig. 9D showed the selected curves of tan δ. Overall, the mechanical property of EP was not impacted greatly within 5 wt% loading P-FRs.

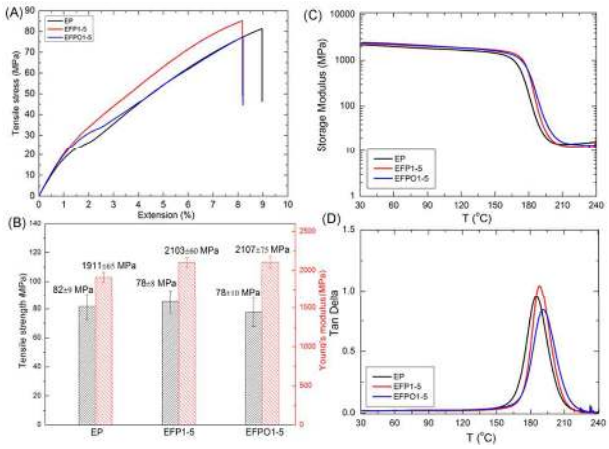

Fig. 9 (A) Strain-stress curves, (B) Charts of tensile strength and Young's modulus (A) of EP, EFP1-5 and EFPO1-5; (C) Storage modulus and (d) Tan δ curves of EP, EFP1-5 and EFPO1-5 from DMA test

4. Conclusions

In this work, two series of phenylphosphonate-based (PO-Ph) and phenylphosphoric-based (PO-OPh) flame retardants (FPx and FPOx, x=1, 2 and 3) were synthesized successfully with high yields. The remarkable exothermic phenomena and the decreased of R (i(epoxy group)/i(ether group)) ratios of EPC/FP1 and EPC/FPO1 revealed N-H group on the structures of synthesized P-FRs was reactive with epoxy group on the structures of EPC during 100 to 220 °C. It indicated that synthesized P-FRs was chemically bonded with EP during curing procedure. Interesting findings between FPx and FPOx (x=1, 2 and 3) on improving flame retardancy of EP (DGEBA-type epoxy resin/DDS system) were showed in different fire tests. FPOx (x= 1. 2 and 3) showed almost no effect on self-extinguishing ability of EP, while FPx (x= 1. 2 and 3) endowed EP with strong self-extinguishing ability within small loadings in UL 94 test. The addition of FPO1 made EP pass V-1 with a high loading of 30 wt%, while EFP1-3 already passed V-1 rating and EFP1-5 passed V-0 rating only with 5 wt% loading (P content lower than 0.7 wt%). In addition, FPx (x= 1. 2 and 3) increased LOI and decreased pHRR of EP in greater way than FPOx (x= 1. 2 and 3) did in cone calorimeter test. Comparing flame-retardant mechanisms, both FP1 and FPO1 acted via accumulating char formation in the condensed phase of EP. Intumescent char residues formed owing to the following conditions in cone calorimeter test of EFP1-5 and EFPO1-5: the acid compounds (H_3PO_3 and H_3PO_4) from thermal decomposition of FP1 and FPO1 acted as acid sources; EP matrix acted as char former; the gaseous products from thermal decomposition of EFP1 and EFPO1 acted as blower. However, FP1 showed flame inhibition in gas phase caused by the produced PO· radical during thermal decomposition of FP1, whereas FPO1 did not show any effect in gas phase. Furthermore, the results of online temperature detection experiment for NTST and ST in UL 94 test showed that flame inhibition effect was the main factor to endow EP with strong self-extinguishing ability in UL 94 test. Moreover, the small loading addition of FP1 and FPO1 present negligible impact on tensile strength, storage modulus and Tg of EP.

View Article Online
DOI: 10.1039/C6RA13168A

Acknowledgements:

One of our authors (Ms. Xiaomin Zhao) would thank the financial support from China Scholarship Council. In addition, this work is partly funded by Ramón y Cajal grant (RYC-2012-10737) and the European Commission under the 7th Framework Program (Marie Curie Career Integration Grant, GA-321951).

Reference

1 C. May, *Epoxy resins: chemistry and technology*, CRC press, 1987.
2 H. Q. Pham and M. J. Marks, *Kirk-Othmer Encyclopedia of Chemical Technology*, 2004.
3 X. Zhang, Q. He, H. Gu, H. A. Colorado, S. Wei and Z. Guo, *Acs Applied Materials & Interfaces*, 2013, **5**, 898-910.
4 H. Gu, J. Guo, Q. He, S. Tadakamalla, X. Zhang, X. Yan, Y. Huang, H. A. Colorado, S. Wei and Z. Guo, *Industrial & Engineering Chemistry Research*, 2013, **52**, 7718-7728.
5 L.-J. Qian, L.-J. Ye, G.-Z. Xu, J. Liu and J.-Q. Guo, *Polymer Degradation and Stability*, 2011, **96**, 1118-1124.
6 T. Mariappan, Y. Zhou, J. Hao and C. A. Wilkie, *European Polymer Journal*, 2013, **49**, 3171-3180.
7 B. Perret, B. Schartel, K. Stöß, M. Ciesielski, J. Diederichs, M. Döring, J. Krämer and V. Altstädt, *European Polymer Journal*, 2011, **47**, 1081-1089.
8 X. Wang, Y.-T. Pan, J.-T. Wan and D.-Y. Wang, *RSC Advances*, 2014, **4**, 46164-46169.
9 M. Rakotomalala, S. Wagner and M. Doering, *Materials*, 2010, **3**, 4300-4327.
10 K. Wu, L. Song, Y. Hu, H. Lu, B. K. Kandola and E. Kandare, *Progress in Organic Coatings*, 2009, **65**, 490-497.
11 M. Gao, W. Wu and Y. Yan, *Journal of Thermal Analysis and Calorimetry*, 2009, **95**, 605-608.
12 J. Artner, M. Ciesielski, O. Walter, M. Doering, R. M. Perez, J. K. W. Sandler, V. Altstaedt and B. Schartel, *Macromolecular Materials and Engineering*, 2008, **293**, 503-514.
13 M. Hou, W. Liu, Q. Su and Y. Liu, *Polymer journal*, 2007, **39**, 696-702.
14 U. Braun, A. I. Balabanovich, B. Schartel, U. Knoll, J. Artner, M. Ciesielski, M. Döring, R. Perez, J. K. Sandler and V. Altstädt, *Polymer*, 2006, **47**, 8495-8508.
15 S. V. Levchik and E. D. Weil, *Polymer International*, 2004, **53**, 1901-1929.
16 G. H. Hsiue, Y. L. Liu and H. H. Liao, *Journal of Polymer Science Part A: Polymer Chemistry*, 2001, **39**, 986-996.
17 C.-S. Wang and J.-Y. Shieh, *Polymer*, 1998, **39**, 5819-5826.
18 R. Perez, J. Sandler, V. Altstädt, T. Hoffmann, D. Pospiech, M. Ciesielski and M. Döring, *Journal of materials science*, 2006, **41**, 341-353.
19 F. Laoutid, L. Bonnaud, M. Alexandre, J.-M. Lopez-Cuesta and P. Dubois, *Materials Science and Engineering: R: Reports*, 2009, **63**, 100-125.
20 S. Yang, J. Wang, S. Huo, L. Cheng and M. Wang, *Polymer Degradation and Stability*, 2015, **119**, 251-259.
21 L. S. Birnbaum and D. F. Staskal, *Environmental health perspectives*, 2004, **112**, 9.
22 P. O. Darnerud, *Environment international*, 2003, **29**, 841-853.
23 K. A. Salmeia and S. Gaan, *Polymer Degradation and Stability*, 2015, **113**, 119-134.
24 S.-Y. Lu and I. Hamerton, *Progress in Polymer Science*, 2002, **27**, 1661-1712.
25 C. A. de Wit, *Chemosphere*, 2002, **46**, 583-624.
26 P. Eriksson, E. Jakobsson and A. Fredriksson, *Environmental health perspectives*, 2001, **109**, 903.
27 D. Enescu, A. Frache, M. Lavaselli, O. Monticelli and F. Marino, *Polymer Degradation and Stability*, 2013, **98**, 297-305.
28 J. Ye, G. Liang, A. Gu, Z. Zhang, J. Han and L. Yuan, *Polymer Degradation and Stability*, 2013, **98**, 597-608.
29 A. S. Keller, N. P. Raju, T. F. Webster and H. M. Stapleton, *Environmental science & technology letters*, 2014, **1**, 152-155.
30 M.-J. Kim, I.-Y. Jeon, J.-M. Seo, L. Dai and J.-B. Baek, *ACS nano*, 2014, **8**, 2820-2825.
31 G. H. Hsiue, Y. L. Liu and H. H. Liao, *Journal of Polymer Science Part A: Polymer Chemistry*, 2001, **39**, 986-996.
32 Z. Li and R. Yang, *Polymer Degradation and Stability*, 2014, **109**, 233-239.
33 G. You, Z. Cheng, H. Peng and H. He, *Journal of Applied Polymer Science*, 2014, **131**.
34 B. Schartel, B. Perret, B. Dittrich, M. Ciesielski, J. Krämer, P. Müller, V. Altstädt, L. Zang and M. Döring, *Macromolecular Materials and Engineering*, 2015.
35 L. Qian, Y. Qiu, J. Liu, F. Xin and Y. Chen, *Journal of Applied Polymer Science*, 2014, **131**.
36 D. Sun and Y. Yao, *Polymer Degradation and Stability*, 2011, **96**, 1720-1724.
37 J. Sun, X. Wang and D. Wu, *ACS applied materials & interfaces*, 2012, **4**, 4047-4061.
38 L. Hetherington, B. Greedy and V. Gouverneur, *Tetrahedron*, 2000, **56**, 2053-2060.
39 X. Lopez, C. Sarasola, A. Largo, C. Barrientos, J. M. Ugalde and B. Lecea, *The Journal of Physical Chemistry*, 1993, **97**, 4078-4079.
40 B. Schartel, *Materials*, 2010, **3**, 4710-4745.
41 R. Dupretz, G. Fontaine, S. Duquesne and S. Bourbigot, *Polymers for Advanced Technologies*, 2015, **26**, 865-873.
42 F. Kempel, B. Schartel, J. M. Marti, K. M. Butler, R. Rossi, S. R. Idelsohn, E. Oñate and A. Hofmann, *Fire and Materials*, 2015, **39**, 570-584.

View Article Online
DOI: 10.1039/C6RA13168A

Graphical Abstract